Surface & Coatings Technology 517 (2025) 132820

Contents lists available at ScienceDirect

Surface & Coatings Technology

journal homepage: www.elsevier.com/locate/surfcoat

The role of ZnAl hydrotalcite conversion layers in corrosion protection of acrylic coating on electrogalvanized steel☆

Thu Thuy Pham [a,b,1], Anh Son Nguyen [a,1], Yoann Paint [c], Thuy Duong Nguyen [a], Thi Xuan Hang To [a], Marie-Georges Olivier [b,c,*]

[a] Institute of Materials Science, Vietnam Academy of Science and Technology, 18 Hoang Quoc Viet, Cau Giay, Hanoi, Viet Nam
[b] Université de Mons, Materials Science Department, Place du Parc 20, Mons, Belgium
[c] Materia Nova, Parc Initialis, Mons, Belgium

ARTICLE INFO

Keywords:
Hydrotalcite
Layered double hydroxide (LDH)
Electrogalvanized steel
Conversion layer
Organic coating

ABSTRACT

ZnAl hydrotalcite (HT) conversion layers were formed on electrogalvanized (EG) steel surfaces at room temperature for two different durations and evaluated as surface treatments. Fourier-transform infrared spectroscopy (FT-IR), X-ray diffraction (XRD), and scanning electronic microscopy with energy-dispersive X-ray spectroscopy (SEM/EDS) confirmed the formation of ZnAl HT hexagonal crystallites, which were formed as a continuous layer on EG steel surface under varying synthesis durations. Polarization curve analysis and electrochemical impedance spectroscopy (EIS) demonstrated that the HT layers improved the corrosion protection of the EG steel substrate. Notably, the HT layer formed with a longer duration exhibited better corrosion resistance. To evaluate the influence of HT layers on the adhesion and corrosion resistance of applied organic coatings, an acrylic coating was applied over the HT-treated surfaces and subjected to pull-off tests, salt spray testing, EIS, and local electrochemical impedance spectroscopy (LEIS). Results showed that the HT layers significantly enhanced adhesion between the EG steel substrate and the acrylic coating, and the acrylic systems with HT layers effectively mitigated corrosion of the EG steel. However, the HT layer formed with a shorter duration exhibited a superior influence on the barrier property and adhesion of the acrylic coating.

1. Introduction

Given their more negative corrosion potential compared to iron, zinc and its alloys are extensively used as sacrificial anodic coatings (galvanized coatings) to protect steel substrates in the transport and construction industries [1]. However, due to the high electrochemical reactivity of zinc, its corrosion rate can be extremely high under atmospheric conditions, forming a loosely bound corrosion product commonly referred to as white rust [2–4]. Recently, polymer coatings have been employed to extend the longevity of galvanized coatings [5–7]. The zinc coatings inherently exhibit limited adhesion strength to polymer coatings [8]. For this reason, applying a pretreatment or conversion layer is essential to modify the surface chemical properties of zinc coatings, enhancing their adhesion strength to polymer coatings and subsequently improving the corrosion protection of the materials.

Chromate and phosphate conversion coatings are extensively employed to provide strong adhesion between the substrate and polymer coatings, as well as protect zinc surface due to their self-healing capability, effective corrosion resistance, and straightforward application [9–11]. In traditional pretreatment, the chromate coatings contain elevated levels of Cr^{6+} salts, which pose a significant risk of toxicity and carcinogenic effects [12]. The application of phosphate conversion coatings also presented several limitations, including the necessity for an additional pore-sealing step and frequent removal of sludge byproducts [13,14]. Furthermore, the phosphating process typically operates at elevated temperatures, leading to increased energy consumption and associated costs [13]. Various pretreatment/conversion layers, including those based on molybdate, silane, rare earth metals, and hydrotalcite (HT), have been suggested in place of chromate and phosphate conversion coatings [9,15–17].

Hydrotalcite, also known as a layered double hydroxide, is an anionic clay characterized by a highly tunable brucite-like layered

☆ This article is part of a Special issue entitled: 'Women in SCT' published in Surface & Coatings Technology.

* Corresponding author at: Université de Mons, Materials Science Department, Place du Parc 20, Mons, Belgium.
E-mail address: marjorie.olivier@umons.ac.be (M.-G. Olivier).

[1] These authors contributed equally to this work.

https://doi.org/10.1016/j.surfcoat.2025.132820
Received 17 July 2025; Received in revised form 9 October 2025; Accepted 15 October 2025
Available online 20 October 2025

structure. The HT structure includes octahedral holes in a brucite-like layer, hosting divalent (M^{2+}) and trivalent/tetravalent (M^{3+}/M^{4+}) cations, and the anions (A^{n-}) are located in main hydration layers to charge equilibrium [18–21]. Through intercalation, anionic corrosion inhibitors can be incorporated into the nanoscale interlayer galleries of HTs [22,23]. The resulting inhibitor-loaded HTs act as nanocontainers capable of storing and gradually releasing inhibitors in a sustained and controlled fashion. In addition, the HT can entrap aggressive ions like Cl^- within the interlayer region, decreasing Cl^- ions concentration between HT interface and surface of substrates, subsequently reducing the metal's corrosion rate [18,23]. Another advantage is that HTs can be directly grown on metallic substrates, forming adherent protective layers via relatively simple synthesis routes [21,24,25]. Recently, in situ growth techniques have been explored for the fabrication of HT-based conversion layers, enabling the development of uniform, strongly bonded layers with enhanced barrier and self-healing properties [26,27].

The methods, such as in-situ growth and hydrothermal treatments, were investigated to apply HT layers on zinc alloys [28–32]. Zheludkevich et al. created ZnAl-NO_3 HT layers on pure zinc substrate by immersing the metal in mixture solution containing both $Al(NO_3)_3$ and $NaNO_3$ (pH 3.2) at 90 °C using a one-step synthesis route [30,33]. Their results elucidated the time-dependent growth mechanism of HT layers and established a clear correlation between reaction duration and surface characteristics. The study demonstrated that a continuous, well-developed HT layer fully covering the zinc surface formed after approximately 20 h of treatment. Hoshino et al. investigated the formation of ZnAl-CO_3 HT layers on EG steel substrates using $Na_2Al_2O_4$-based solutions containing KNO_3, NH_4NO_3, and $Zn(NO_3)_2$, with the solution pH ranging from 11.5 to 13.3 for 16 h at room temperature [28]. They reported that both the growth behavior and the protective performance of the HT layers were strongly governed by the pH of the precursor solution. Their results revealed that corrosion resistance improved with increasing pH up to ~12.6, beyond which excessive alkalinity led to ZnO formation and a consequent decline in protection. An interesting aspect is that the formation mechanism of HT differs fundamentally between acidic and alkaline environments: in acidic media, $ZnOH^+$ and $Al(OH)_4^-$ acted as the main precursors, whereas in alkaline solutions the process was dominated by $Zn(OH)_3^-$ and $Al(OH)_4^-$ species [28,30]. Consequently, the nucleation and subsequent crystal growth pathways differ under these two conditions, leading to distinct HT morphology. Amanian et al. systematically examined the influence of processing duration, with immersion times ranging from 2 to 24 h, on the formation of ZnAl-CO_3 HT layers on EG steel and their subsequent effect on corrosion resistance and adhesion of epoxy-polyamide coatings [8,34]. Their findings demonstrated that extending the treatment time up to an optimal duration of approximately 16 h significantly enhanced corrosion protection and the adhesion of top coating. This improvement was attributed to the growth of HT nanosheets, which increased surface roughness and thereby promoted stronger mechanical interlocking at the polymer–metal interface. However, they also observed that excessively prolonged treatment times adversely affected performance. In particular, overgrowth of HT led to excessive surface roughness and wettability, which reduced barrier effectiveness and, consequently, corrosion resistance.

In our previous studies, the ZnAl-CO_3 HT layers were synthesized on different zinc alloy coated steel substrates by immersing the samples in a mixed aqueous solution containing $Al(NO_3)_3$ and $Zn(NO_3)_2$ at pH 12 and room temperature [29,35]. The results demonstrated that these HT layers acted as effective protective barriers, capable of delaying substrate corrosion by impeding the ingress of aggressive species. Similar to other studies on the synthesis of ZnAl-CO_3 HT layers in alkaline environments [8,28], the preparation process in our work was relatively time-consuming, with a total synthesis duration of approximately 22 h, which may represent a limitation for the practical application of this approach. Moreover, the resulting HT layers were relatively thick and porous, which could reduce their efficiency in improving the corrosion resistance and adhesion of subsequent organic coatings. Therefore, the present study aims to shorten the HT layer preparation time on EG steel substrates to 7 h and to compare the resulting structure and corrosion resistance with those obtained from the conventional 22 h treatment. In addition, this work specifically investigates the influence of HT layers on the adhesion and corrosion protection of organic coatings. To contribute to the HT treatment more evidently, an acrylic coating is selected as the topcoat because of its comparatively weaker barrier performance than more robust systems such as epoxy or polyurethane. This strategy allows the role of the HT interlayer in enhancing coating performance to be more clearly identified.

2. Materials and methods

2.1. Materials

The organic coating is Diial BR 116 acrylic resin from Mitsubishi, dissolved in xylene. The xylene content is 60 %. All chemicals employed in this investigation are of analytical quality, including: NaOH, NaCl, $Al(NO_3)_3{\cdot}9H_2O$, $Zn(NO_3)_2{\cdot}7H_2O$, $ZnCl_2$, and NH_4Cl.

XC35 carbon steel specimens (60 × 40 × 2 mm) were employed as substrates for electrogalvanized steel. The chemical composition of the substrate was (wt%): C 0.35, Mn 0.65, Si 0.25, P 0.035, S 0.035, with Fe as the balance [36].

2.2. Electrogalvanized steel preparation

The investigated substrate was electrogalvanized (EG) steel, prepared from XC35 carbon steel specimens. The samples were cleaned in a 60 g/L UDYPREP-110EC solution at 60 °C for 10 min, rinsed with water, and subsequently immersed in a 10 % HCl solution for 3 min before zinc electroplating [37]. The electrodeposition process used two platinum-coated titanium counter electrodes. Zinc electroplating was performed in an electrolyte bath composed of $ZnCl_2$ (60 g/L) and NH_4Cl (250 g/L), with the pH solution controlled within the range of 5–5.5. Electrolysis was carried out at a direct current density of 2 A/dm^2 at room temperature for 40 min. The roughness and thickness of the zinc deposit were 1.0 ± 0.1 μm and 10.0 μm, respectively.

2.3. Preparation ZnAl HT layers on EG steel substrates

Before preparing ZnAl HT layers, the EG steel substrates were treated with ultrasonic agitation in acetone for 30 min and washed with commercial Gardoclean alkaline solution, ethanol, and distilled water [29]. The HT layers synthesis was carried out at room temperature. The solution baths were created by dissolving and stirring 0.05 M $Al(NO_3)_3$ with 0.2 M NaOH in distilled water, followed by addition of 0.03 M $Zn(NO_3)_2$. The pH of mixture reaction was set to 12 by adding 1 M NaOH. The HT layers were synthesized by immersing EG steel substrates in precursor baths under two different conditions. For the HT-1 layer, the substrates were immersed for 2 h under continuous stirring, followed by 5 h without agitation. For the HT-2 layer, immersion was carried out for 6 h under stirring and followed by 16 h of static immersion. The total process duration of HT-1 was reduced from 15 h to HT-2. The produced HT layers were cleaned with distilled water and subsequently dried at 70 °C.

2.4. Preparation of acrylic coatings

The acrylic resin was stirred with xylene for 24 h before applying it to EG steel without and with HT layers. The acrylic coatings were applied by using spin-coating technique (350 rpm for 20 s) and then dried naturally at room temperature for two weeks. The dried coating thickness was determined at around 32 ± 5 μm (assessed by utilizing Minitest 600 Erichen digital meter).

2.5. Methods

FTIR spectra of the HT layers were recorded using a Nexus 670 Nicolet spectrometer in the wavenumber range of 4000–500 cm^{-1} at room temperature. The structure of HT layer samples was studied by XRD, which was collected by Siemens diffractometer D5000 using CuKα radiation (0.15406 nm) in the 2θ range from 2° to 70° with a rate of 2.6° min^{-1}. The morphology and elemental composition of the EG steel and HT layers were examined using Field Emission Scanning Electronic Microscope (FE-SEM, Hitachi SU8020) equipped with an energy dispersive X-ray spectroscopy (EDS) system.

The optical photographs of acrylic coating on EG steel in the absence and presence of HT layers were observed by Keyence VH-Z100 3D digital microscope. The adhesion strength for all acrylic coating systems was evaluated using a pull-off test (following ASTM D4541 standard) and the cross-hatch adhesion test in accordance with ASTM D3359 (Elcometer 1542). Salt spray testing was conducted on intact acrylic coating systems using a QFOGCCT-600 chamber, following ASTM B117 standards.

Electrochemical behavior of EG steel and HT layers immersed in 0.1 M NaCl was investigated by using EIS and polarization curves. The electrochemical tests were recorded by a Biologic VSP300 apparatus using a classical three-electrode cell, comprising a platinum counter electrode, an Ag/AgCl (saturated KCl) reference electrode, and the sample as the working electrode (exposed area = 1 cm^2). Before each test, the samples were immersed for 15 min to stabilize the open-circuit potential (OCP). The EIS measurements were performed over a frequency range of 100 kHz to 10 mHz using 50 points and a sinusoidal perturbation of 10 m*V* (peak-to-peak). Polarization scans were recorded from 0.03 V to −0.40 V and from −0.03 to 0.40 V (vs. OCP (V/Ag/AgCl)) with a scan rate of 0.2 mV s^{-1}. The corrosion protection of acrylic coating systems was evaluated in 3.0 wt% NaCl by EIS. The same experimental conditions were employed for EIS measurements on uncoated samples; however, the acrylic coating systems were studied with an exposed area of 7.06 cm^2, using 6 points per decade with 30 mV of amplitude. The measurements were performed in triplicate to ensure reproducibility.

LEIS techniques were utilized to evaluate the active corrosion properties of acrylic coating systems. Measurements were performed using a Biologic M470 scanning electrochemical workstation. Sample preparation involved introducing an artificial scratch of 100 ± 10 μm to each coated surface. The experimental setup comprised a five-electrode configuration within a 1 mM NaCl solution. A carbon circular grid, functioning as the counter-electrode, encircled the 10 mm × 10 mm region of interest. An Ag/AgCl (saturated KCl) reference electrode was positioned proximally to the analyzed area. A platinum bi-electrode probe was precisely positioned approximately 200 μm ± 50 μm above the sample surface and moved across the analyzed region with a step size of 500 μm in both x and y directions. LEIS mappings were acquired at frequencies of 1 kHz and 1 Hz from two separate locations on the same sample.

3. Results and discussion

3.1. Characterization and morphology of ZnAl HT layers

The XRD patterns of synthesized HT layers are presented in Fig. 1. The patterns of all HT layer samples at around 11.66°, 23.58°, and 34.60° corresponded to (003), (006), and (012) reflection peaks, respectively, which were characteristic of HT structure intercalated with carbonate (JCPDS No. 48–1022). The intensity of HT-2 characteristic peaks was significantly higher than that of HT-1 ones, indicating a greater quantity of deposited HT crystals on EG steel surface with extended reaction durations. In addition, the reflections attributed to zinc oxide (ZnO) peaks cannot be observed for both samples.

The structure of ZnAl HT layers was confirmed by the FT-IR spectroscopy (Fig. 2). The broad absorption band around 3400 cm^{-1} was

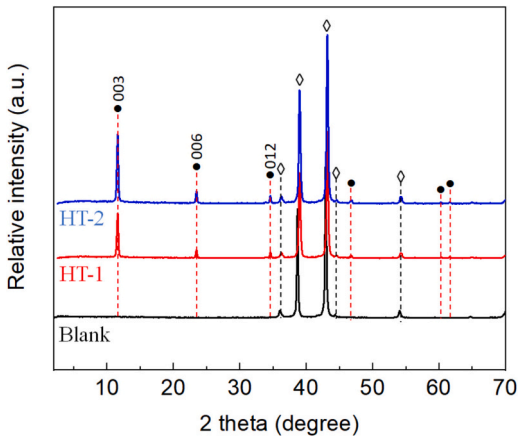

Fig. 1. XRD patterns of EG steel, HT-1 and HT-2 samples. ●: HT and ◊: zinc.

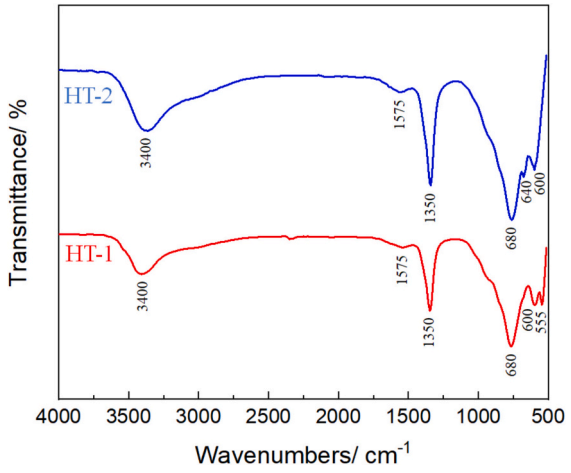

Fig. 2. The FTIR spectra of HT-1 and HT-2 samples.

assigned to O—H stretching vibration of interlayer water molecules and metal hydroxyl groups, and the peaks near 1575 cm^{-1} corresponded to the bending vibration of water molecules [34,35]. The 1350 cm^{-1} characteristic peak was related to C—O stretching vibration, confirming the presence of carbonate ions in HT interlayer [15,28]. The bands appearing from 800 to 500 cm^{-1} were associated with vibrational modes of M-O, M-OH, M-O-M, and O-M-O (M: Zn and Al) [15,35].

The morphology of bare EG steel substrate and prepared HT layers with different reaction time is shown in Fig. 3. It is clear that two HT layers exhibited a hexagonal crystal structure when grown on the substrate surface, consistent with our previous findings [29,35]. Fig. 3.b2 and c2. showed that the HT-2 hexagonal crystallites exhibited a notably larger size compared to those of HT-1. The crystallites of both HT-1 and HT-2 close to surfaces were arranged in an alternating staggered pattern (Fig. 3.b1 and c1), however, the HT-2 layer, which was larger, exhibiting a slanted stagger, and demonstrating greater uniformity, was expected to offer enhanced effectiveness in preventing the penetration of aggressive ions and protecting the substrate from corrosive environments. The EDS results (Table 1) showed that the HT layers primarily consisted Zn, O, and Al elements, with variations in their distribution across the examined areas. As the extended reaction duration, there was a reduction in the Zn content, accompanied by an increase in the percentages of Al and O, suggesting a growth in the thickness of HT conversion layer.

Fig. 4 shows cross-sections of HT layers at various treatment times, demonstrating that the treatment duration influenced the thickness of the HT layers. Longer treatment time resulted in increased HT layer

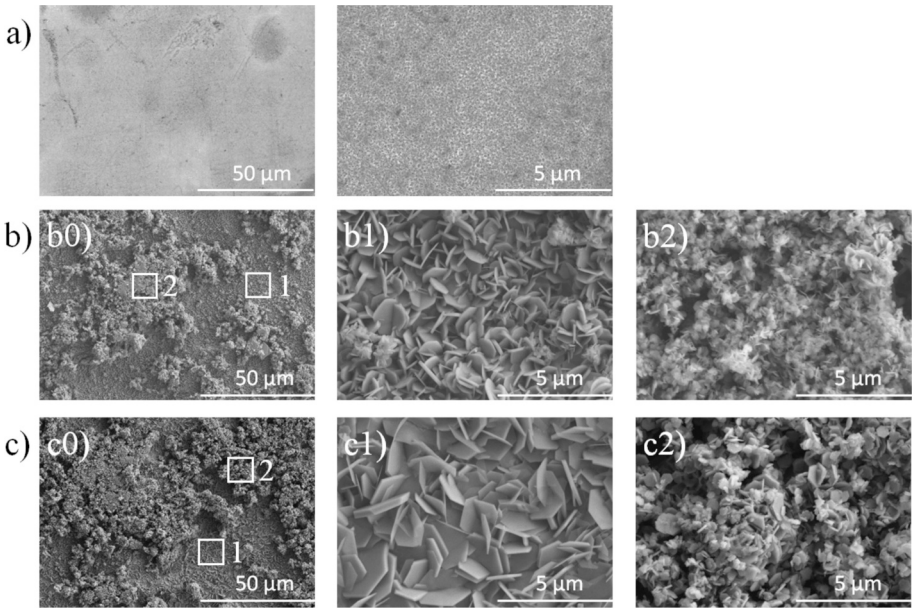

Fig. 3. SEM images of EG steel (a), HT-1 (b), and HT-2 (c) samples.

Table 1
EDS test results of EG steel and HT samples.

Sample	Element content (wt%)			
	Zn	Al	O	C
EG	96.6 ± 1.5	–	1.5 ± 0.2	1.9 ± 0.2
HT-1 1	77.2 ± 1.4	2.9 ± 0.3	17.8 ± 0.5	2.1 ± 0.1
HT-1 2	54.7 ± 1.1	6.6 ± 0.4	36.2 ± 0.9	2.5 ± 0.2
HT-2 1	70.8 ± 1.3	6.4 ± 0.4	20.6 ± 0.7	2.2 ± 0.1
HT-2 2	47.1 ± 1.0	10.2 ± 0.5	40.3 ± 1.1	2.4 ± 0.2

thickness. However, visible gaps were observed within the HT layer's cross-sections, which may reduce their effectiveness in providing anti-corrosion.

3.2. Corrosion protection of the ZnAl HT layers

The polarization curves (Fig. 5) indicated that the samples with ZnAl HT layers exhibit lower anodic and cathodic current densities compared to the bare sample. Rather similar cathodic current densities were measured for HT-1 and HT-2 samples (slightly lower with the HT-2 layer). At −1.2 *V* of corrosion potential, the current density values for the HT-1 and HT-2 layers were 2.05×10^{-5} and 1.65×10^{-5} A·cm^{-2}, respectively. However, the HT-2 layer exhibited significantly lower anodic current densities compared to the HT-1 layer. At a corrosion potential of −0.8 V, the current density value for the HT-2 layer was 1.85×10^{-4} A·cm^{-2}, notably lower than the 5.89×10^{-4} A·cm^{-2} recorded for the HT-1 layer. The decrease in polarizing current for the HT-treated samples suggested that the ZnAl HT conversion layers enhanced the anti-corrosion of the EG steel substrates. Among these, the ZnAl HT-2 sample showed the lowest current density, implying that a longer HT treatment duration can further inhibit corrosion of EG steel substrate.

Fig. 6. presents Nyquist and Bode plots for EG steel and HT layer samples after 24 h in 0.1 M NaCl. For bare EG steel, two time constants (TCs) were observed, and the EIS data were accordingly fitted using the equivalent electrical circuit (EEC) shown in Fig. 7.a. Specifically, the medium frequency TC can be related to the native zinc oxide/hydroxide layer deposited on surface of bare substrate as corrosion products in chloride-containing corrosive environment [35,38], and was

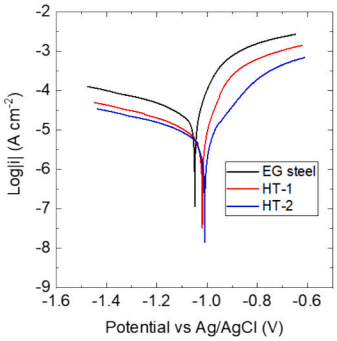

Fig. 5. Polarization curves of EG steel and HT samples after 24 h in 0.1 M NaCl.

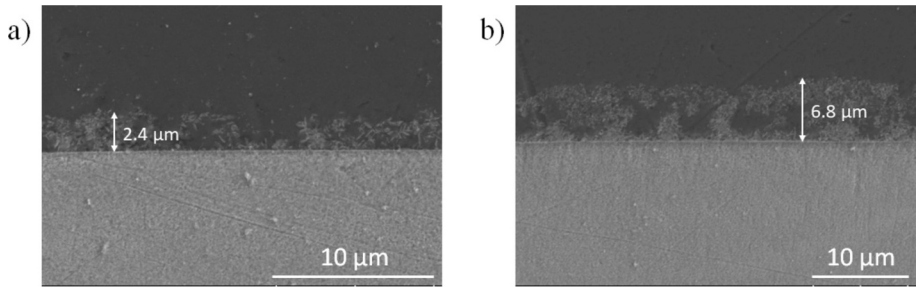

Fig. 4. SEM of the cross-sections of HT-1 sample (a) and HT-2 sample (b).

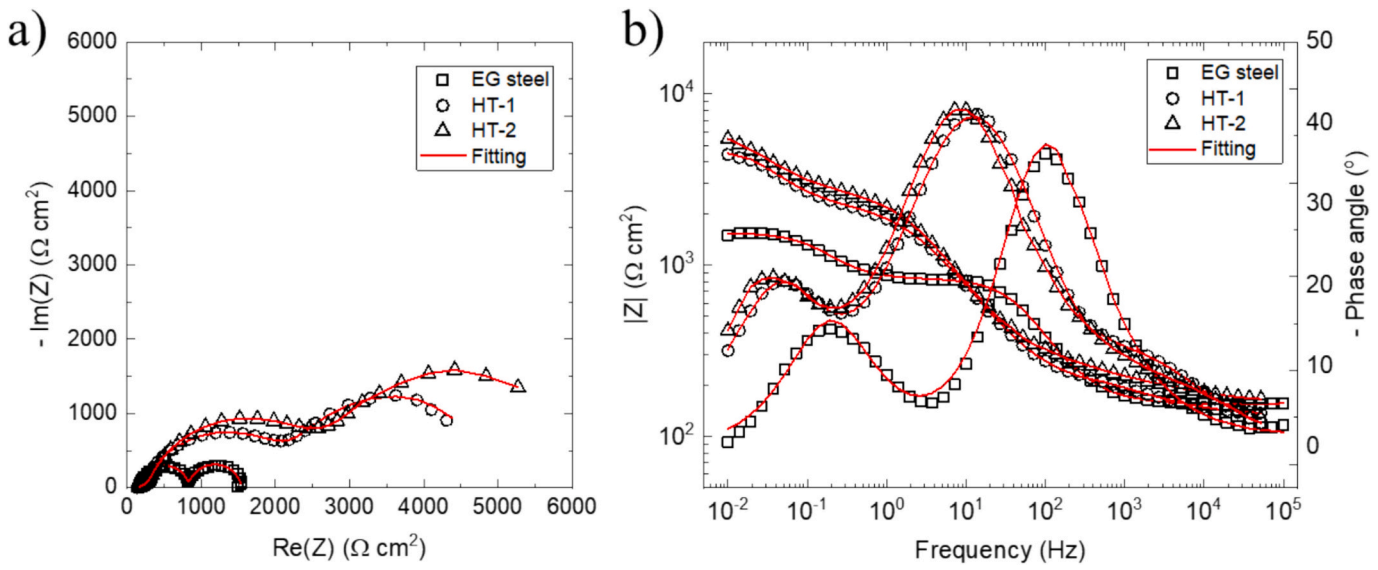

Fig. 6. EIS results of EG steel and HT samples after 24 h in 0.1 M NaCl solution: Nyquist plot (a) and Bode plot (b).

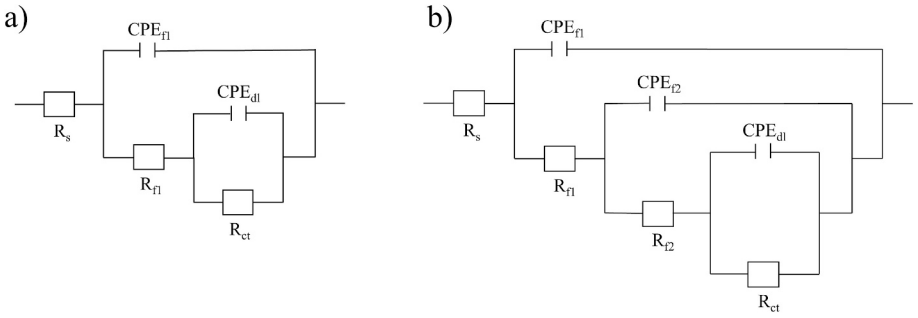

Fig. 7. EEC models used for fitting the EIS data of EG steel and HT samples.

represented by R_{f1} and CPE_{f1}. The second TC, appearing at lower frequencies, corresponded to electrochemical processes occurring at the metal/electrolyte interface. It is modeled by the double layer constant phase element (CPE_{dl}) in parallel with the charge transfer resistance (R_{ct}). Consistent with our previous studies, three TCs can be identified in the impedance spectra of the HT layers (Fig. 7.b) [15,29,35]. In this model, R_s, R_{f1}, R_{f2}, and R_{ct} corresponded to solution resistance, resistance of oxide layer, resistance of HT layer, and charge transfer resistance, respectively. Similarly, CPE_{f1}, CPE_{f2}, and CPE_{dl} were associated with the capacitance of the oxide layer, HT layer, and double layer, respectively.

The resistance values of R_{f1} and R_{f2} for HT-2 sample were 106 and 2805 Ω·cm^2, respectively, which were slightly higher than those recorded for HT-1 sample (78 and 2206 Ω·cm^2). Moreover, the CPE values associated with the capacitance of oxide layer (2.02×10^{-5} $\Omega^{-1}\cdot s^n\cdot cm^{-2}$) and HT layer ($9.05 \times 10^{-5}$ $\Omega^{-1}\cdot s^n\cdot cm^{-2}$) in the HT-2 sample were smaller than the corresponding values in HT-1 sample (Table 2). The higher R_{f1} and R_{f2} values, along with lower CPE_{f1} and CPE_{f2} values, indicated that the HT-2 layer was denser and exhibited improved corrosion resistance compared to HT-1 layer. This enhancement can be linked to greater thickness of the HT-2 layer resulting from a longer treatment time (Fig. 4). In general, greater values of $|Z|_{10\ mHz}$ and R_{ct} are indicative of improved corrosion resistance [15,39]. The $|Z|_{10\ mHz}$ values of EG steel, HT-1, and HT-2 samples after 24 h were 1492, 4403, and 5440 Ω·cm^2, respectively (Table 2). Correspondingly, the R_{ct} values were 683, 2751, and 3407 Ω·cm^2 (Table 2). Both HT layers exhibited significantly higher $|Z|_{10\ mHz}$ and R_{ct} values compared to the uncoated EG steel, with the protective performance following the order: HT-2 > HT-1 > EG steel. After 24 h of immersion in 0.1 M NaCl, the $|Z|_{10\ mHz}$ values of the HT-1 and HT-2 layers were lower than those reported for ZnAl-CO_3 HT layers formed on zinc alloy coated steel substrates such as ZnAl and ZnAlMg alloys, indicating comparatively lower corrosion resistance [29]. In contrast, when the HT-2 layer was compared with the HT layer prepared on another EG steel substrate under identical synthesis and electrochemical testing conditions, no significant difference in the $|Z|_{10\ mHz}$ value was observed [35]. This suggests that, for electrogalvanized substrates, the corrosion protection efficiency of the HT layer was not strongly affected by minor variations

Table 2
Results of fitted EIS for EG steel, HT layers samples.

Sample	CPE_{f1} ($\Omega^{-1}\cdot s^n\cdot cm^{-2}$)	n_{f1}	R_{f1} (Ω·cm^2)	CPE_{f2} ($\Omega^{-1}\cdot s^n\cdot cm^{-2}$)	n_{f2}	R_{f2} (Ω·cm^2)	CPE_{dl} ($\Omega^{-1}\cdot s^n\cdot cm^{-2}$)	n	R_{ct} (Ω·cm^2)	$\lvert Z\rvert_{10\ mHz}$ (Ω·cm^2)
EG steel	1.02×10^{-5}	0.88	698	–	–	–	1.32×10^{-3}	0.9	683	1492
HT-1	6.02×10^{-5}	0.65	78	1.43×10^{-4}	0.80	2206	1.20×10^{-3}	0.86	2751	4403
HT-2	2.02×10^{-5}	0.68	106	9.05×10^{-5}	0.81	2805	9.14×10^{-4}	0.88	3407	5440

in the substrate surface characteristics. Interestingly, the $|Z|_{10\ mHz}$ value of the HT-1 layer was similar to that of the ZnAl-CO_3 HT layer synthesized for 8 h in an alkaline medium on EG steel by Amanian et al. [8], which was close to the 7 h synthesis time used in this work. Despite variations in the initial reaction bath conditions, the impedance values indicated that both coatings exhibit a similar level of corrosion resistance. The HT conversion layers improved anti-corrosion of the EG steel, and the longer treatment time further enhanced the corrosion protection offered by the HT layer. These results were consistent with the corrosion resistance trend observed in the polarization curves.

3.3. Corrosion protection of acrylic coating system

Fig. 8. shows the surface of acrylic coatings applied to the bare EG substrate and HT layers. The treatment time of the HT layers was found to influence the morphology of the top acrylic coatings. Compared to the untreated sample, the HT-1 layer did not noticeably alter the surface morphology of the acrylic coatings. Some defects were observed in the HT sample with a longer treatment time. This sample had a higher deposition content and a porous structure, which allowed for a greater dispersion of HT within the acrylic matrix during the application of the organic coating via the spin coating method. This can be responsible for particle agglomeration occurring in certain areas during the formation of the acrylic coating, and subsequently causing defects.

EIS tests (Fig. 9) were conducted to quantitatively assess the anti-corrosion and further investigate the corrosion mechanism of acrylic coating systems immersed in a 3.0 wt% NaCl solution over a 28-day exposure period. Generally, the TC at high frequency corresponded to the response of the coating, while the TC at low and medium frequency was linked to the charge transfer process at the metallic surface beneath the acrylic coating [40,41]. The EG/AC and ZnAl HT-1/AC system exhibited a second TC after 14 days of immersion, confirming that the corrosive medium invades the acrylic coating and then begins to corrode the electrode surface. In contrast, the ZnAl HT-2/AC coating systems displayed two TCs early in the immersion, which were attributed to defects in the acrylic coating that reduced its shielding effectiveness (Fig. 9). To better understand the corrosion behavior of the acrylic coating systems, the EIS results for acrylic coating systems were analyzed using appropriate EEC (Fig. 10). R_s, R_f, and R_{ct} represent the electrolyte resistance, acrylic coating resistance, and charge transfer resistance, respectively. Additionally, constant phase elements (CPE_{dl} and CPE_f) were used in place of ideal capacitance to account for the system's heterogeneity. The CPE_{dl} represented the electric double layer capacitance, while the CPE_f corresponded to the coating capacitance. The impedance values at low-frequency in the Bode plots served as a quantitative measure of the barrier properties of acrylic coating systems (Table 3). At the beginning of immersion, the coating system with HT layers showed a higher low-frequency impedance than the EG/AC sample (Fig. 9). This improvement is attributed to the HT layers, which allow the acrylic resin to wick into and seal microvoids during curing, thereby forming a compact, tortuous interphase that hinders ionic transport [8,42]. The more complex diffusion pathway created by this interphase increases the overall resistance of the coating system. Similar results were reported by Xu et al. [24], they found that the incorporation of an in-situ ZnAl HT layer led to higher initial impedance values owing to its contribution to the overall barrier resistance of the coating system. The $|Z|_{100\ mHz}$ for the acrylic coating system without the ZnAl HT pretreatment layer decreased significantly from 8.89×10^6 to $8.35 \times 10^3\ \Omega{\cdot}cm^2$ throughout the corrosive test, confirming a gradual decline in the barrier performance of acrylic coating on the untreated substrate. Notably, after 14 days of immersion, these values for the EG/AC sample decreased to around $10^4\ \Omega{\cdot}cm^2$, suggesting that the acrylic coating had lost its ability to resist the penetration of corrosive environment. The $|Z|_{100\ mHz}$ values for the ZnAl HT-1/AC and HT-2/AC samples were substantially greater than the corresponding values in EG/AC sample during corrosive test, especially, since the HT-1/AC sample showed the highest $|Z|_{100\ mHz}$ values. These findings indicated that the HT layers substantially enhanced the anti-corrosion performance of the acrylic coating systems. However, the impedance values of acrylic coatings on HT-pretreated substrates also decreased noticeably over time.

The fitting results reveal that the EG/AC sample showed the lowest R_f values and the highest CPE_f compared to the other samples with ZnAl HT-pretreated substrates during the corrosion test (Table 3). This indicates that the acrylic coating on untreated substrate exhibited weak physical barrier properties, allowing water containing corrosive ions to easily penetrate through internal defects to the organic coating/metal interface [24]. During 28 days of immersion, the ZnAl HT-1/AC sample maintained the highest R_f value ($1.51 \times 10^7\ \Omega{\cdot}cm^2$) and the lowest CPE_f value ($1.31 \times 10^{-9}\ \Omega^{-1}{\cdot}s^n{\cdot}cm^{-2}$), indicating that the combination of acrylic resin and HT layer with shorter treated time effectively prevented water penetration and diffusion in corrosive environments. Throughout the test, the EG/AC sample consistently had the highest CPE_{dl} and the lowest R_{ct} values among all coating systems, indicating poor inhibition of corrosion processes at the metal/coating interface. Additionally, the EG/AC sample exhibited a rising trend in CPE_{dl} values during corrosive test, suggesting a gradual delamination of the acrylic topcoat from the zinc substrate [24]. Table 3 showed that the CPE_{dl} values of the acrylic coating systems after 28 days of immersion followed this order: EG/AC ($8.85 \times 10^{-5}\ \Omega^{-1}{\cdot}s^n{\cdot}cm^{-2}$) > ZnAl HT-2/AC ($7.26 \times 10^{-7}\ \Omega^{-1}{\cdot}s^n{\cdot}cm^{-2}$) > ZnAl HT-1/AC ($1.07 \times 10^{-7}\ \Omega^{-1}{\cdot}s^n{\cdot}cm^{-2}$), while the R_{ct} values exhibited the opposite trend. The significantly lower CPE_{dl} values and higher R_{ct} values of the ZnAl HT-1/AC and HT-2/AC samples further confirmed that the HT layers greatly enhanced the adhesion and barrier properties of acrylic coatings and limited the exposed area to the aggressive electrolyte.

Fig. 11. shows the results of a visual inspection of acrylic coating systems after 28 days in 3.0 wt% NaCl. As seen, the acrylic coating system without ZnAl HT layers exhibited severe deterioration. Both "white rust" and "red rust" corrosion products appeared on the EG/AC surface, indicating that the acrylic coating alone offered insufficient protection for the long-term corrosion resistance of EG steel. Pitting corrosion was observed on acrylic coating systems with ZnAl HT layer. The corrosion level of ZnAl HT-1/AC was significantly lower than in HT-2/AC.

LEIS was employed to assess the localized corrosion protection achieved by combining acrylic resin with HT layers. Selecting the appropriate frequency for mapping is crucial, so local impedance measurements were conducted above artificially scratched acrylic coating

Fig. 8. Optical photographs of EG/AC (a), HT-1/AC (b), and HT-2/AC (c) coatings by 3D VH-Z100.

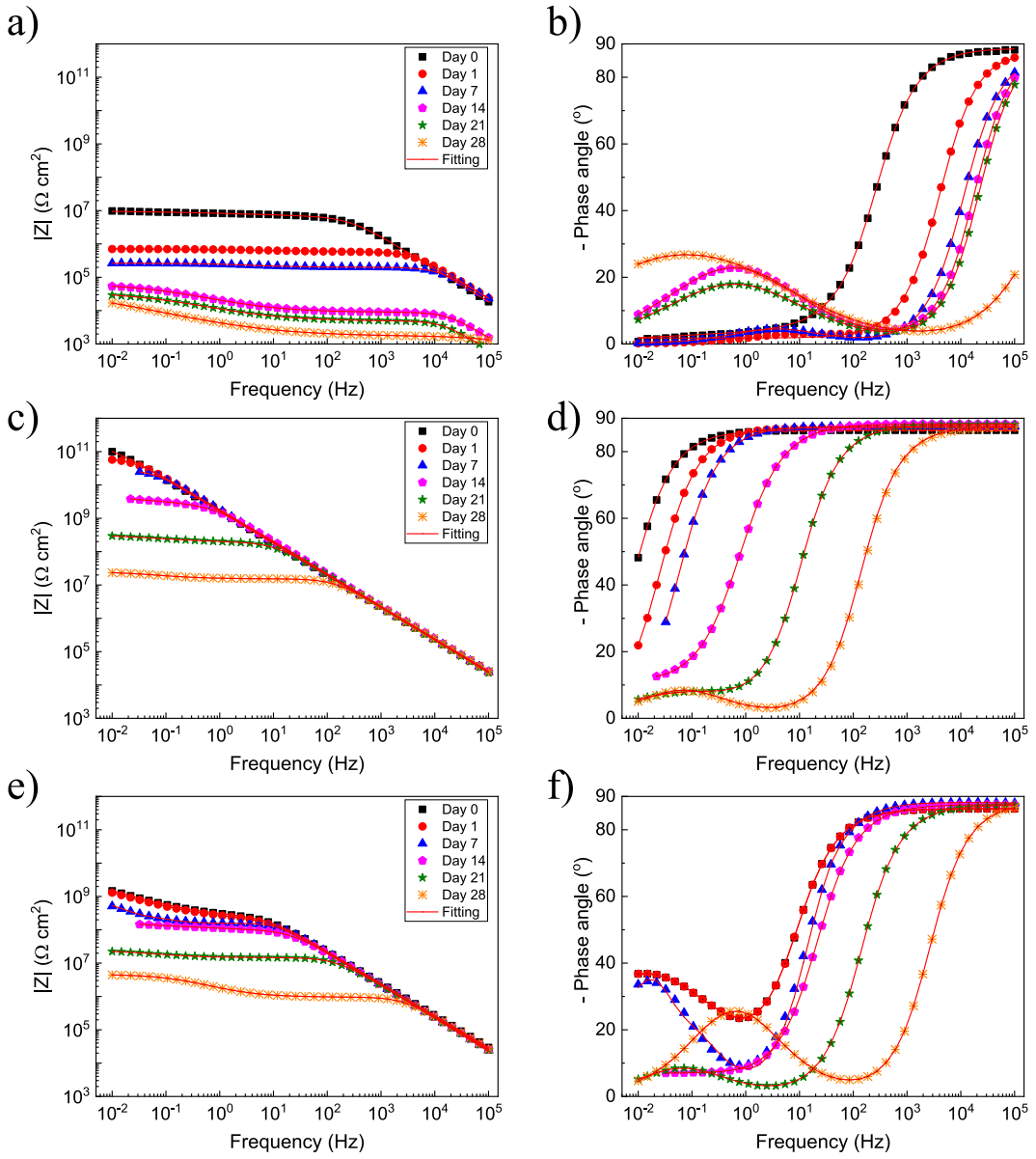

Fig. 9. Bode plots of intact acrylic coating systems immersed in 3.0 wt% NaCl solution: EG/AC (a, b), HT-1/AC (c, d), and HT-2/AC (e, f) samples.

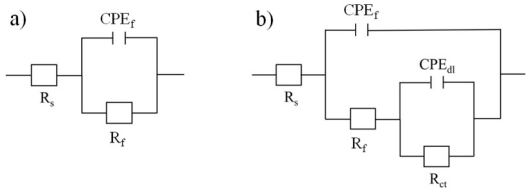

Fig. 10. EEC models used for fitting the EIS data of acrylic coating systems.

systems. High-frequency LEIS data offer valuable insights into the integrity and barrier properties of organic coatings, reflecting their resistance to ionic penetration. In contrast, low-frequency LEIS responses are primarily linked to electrochemical processes at the coating-substrate interface and within defects, providing information about corrosion activity and coating degradation [43].

EIS results revealed that the acrylic coating system incorporating the HT layer synthesized for a shorter duration demonstrated enhanced corrosion resistance relative to the coating system with the longer-treated HT layer. Therefore, the HT-1/AC sample was selected for comparison with EG/AC sample by LEIS method. Fig. 12. shows mappings performed over the scratched area of EG/AC and HT-1/AC samples at 1 kHz after 2 h, 24 h, and 168 h. It can be observed that the admittance of scratched regions was distinctly higher than that of the intact acrylic coating in all samples. For the EG/AC sample, admittance values within the scratched area were higher than those measured in acrylic coating systems with HT pretreatment layers during 168 h of immersion. Additionally, the growing corrosion activity at the damaged area was visible for the EG/AC samples, characterized by increased admittance and size of the scratch on mappings with the immersion time. This indicated the gradual expansion of the scratched region as the corrosive medium penetrated the acrylic coating through artificial defects [40]. In the HT-1/AC sample, the admittance values within the scratch showed a slight increase over the immersion period. A similar trend of gradually increasing corrosion activity at the damaged area was observed in the EG/AC samples. However, the growth of the scratch size in the HT-1/AC sample was significantly less pronounced compared to that in the EG/AC sample.

Mappings performed at 1 Hz for acrylic coating systems during 168 h of immersion are reported in Fig. 13. The results show that the

Table 3
Results of fitted EIS for EG/AC, HT-1/AC, and HT-2/AC samples during 28 days in 3.0 wt% NaCl solution.

Samples	Exposure time (days)	CPE_f ($\Omega^{-1}\cdot s^n\cdot cm^{-2}$)	n_f	R_f ($\Omega\cdot cm^2$)	CPE_{dl} ($\Omega^{-1}\cdot s^n\cdot cm^{-2}$)	n	R_{ct} ($\Omega\cdot cm^2$)	$\|Z\|_{100mHz}$ ($\Omega\cdot cm^2$)
EG/AC	0	1.01×10^{-10}	0.98	9.30×10^{6}	–	–	–	8.89×10^{6}
	1	6.88×10^{-10}	0.97	7.86×10^{5}	–	–	–	6.99×10^{5}
	7	8.91×10^{-10}	0.95	2.71×10^{5}	–	–	–	2.62×10^{5}
	14	9.98×10^{-10}	0.94	8.86×10^{3}	2.40×10^{-6}	0.64	5.53×10^{4}	3.75×10^{4}
	21	1.41×10^{-9}	0.92	5.28×10^{3}	9.33×10^{-6}	0.63	3.12×10^{4}	2.01×10^{4}
	28	2.20×10^{-7}	0.71	1.72×10^{3}	8.85×10^{-5}	0.64	2.66×10^{4}	8.35×10^{3}
HT-1/AC	0	3.05×10^{-11}	0.98	1.63×10^{11}	–	–	–	1.37×10^{10}
	1	6.36×10^{-11}	0.98	6.29×10^{10}	–	–	–	1.50×10^{10}
	7	8.94×10^{-11}	0.97	2.88×10^{10}	–	–	–	1.38×10^{10}
	14	1.01×10^{-10}	0.97	3.36×10^{9}	3.45×10^{-9}	0.69	1.97×10^{9}	3.08×10^{9}
	21	4.93×10^{-10}	0.96	1.97×10^{8}	1.40×10^{-8}	0.66	1.53×10^{8}	2.40×10^{8}
	28	1.31×10^{-9}	0.95	1.51×10^{7}	1.07×10^{-7}	0.66	9.89×10^{6}	1.88×10^{7}
HT-2/AC	0	9.26×10^{-11}	0.98	3.21×10^{8}	3.26×10^{-9}	0.73	3.86×10^{9}	5.59×10^{8}
	1	3.90×10^{-10}	0.97	2.87×10^{8}	3.69×10^{-9}	0.73	2.87×10^{9}	4.94×10^{8}
	7	6.51×10^{-10}	0.97	1.58×10^{8}	1.68×10^{-8}	0.71	6.08×10^{8}	2.04×10^{8}
	14	9.12×10^{-10}	0.96	9.79×10^{7}	1.73×10^{-8}	0.65	1.42×10^{8}	1.32×10^{8}
	21	9.84×10^{-10}	0.95	1.46×10^{7}	2.42×10^{-7}	0.66	9.56×10^{6}	1.79×10^{7}
	28	6.01×10^{-9}	0.94	9.54×10^{5}	7.26×10^{-7}	0.67	3.71×10^{6}	3.53×10^{6}

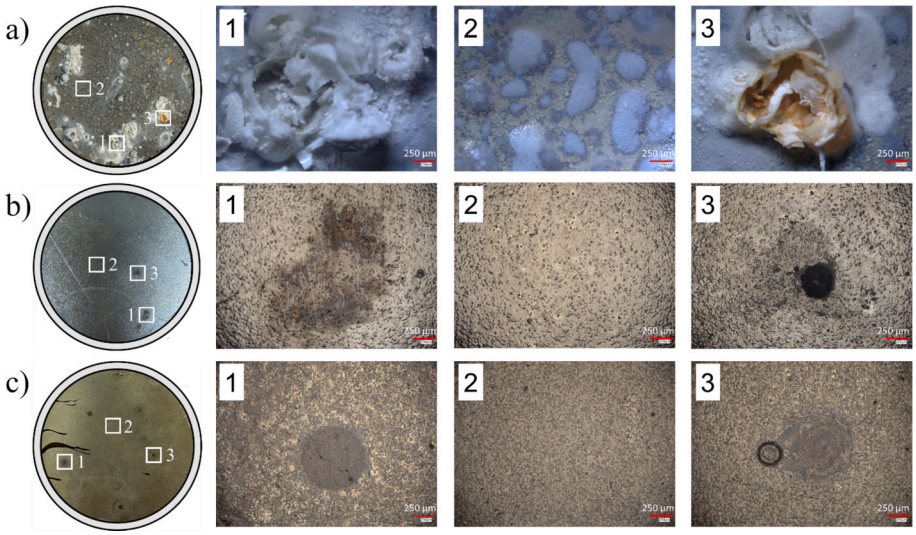

Fig. 11. Optical photographs of (a) EG/AC, (b) HT-1/AC, and (c) HT-2/AC acrylic coating systems after 28 days in 3.0 wt% NaCl solution by 3D VH-Z100.

admittance values over the scratched areas of acrylic coatings with HT layer were significantly lower than those observed for EG/AC samples. A 5–7 order of magnitude increase in admittance was detected at the scratch compared to the surrounding coating. The scratch was visible on the mappings throughout the test. The admittance values for EG/AC and ZnAl HT-1/AC samples increased slightly over time, indicating increased corrosion activity at the defects. However, the admittance values over the scratched areas of acrylic coatings with HT-1 layer were significantly lower than those observed for EG/AC sample. LEIS results indicated that the HT layer increased the corrosion resistance performance in scratched areas.

The adhesion strength for all acrylic coating systems, as determined by the pull-off test (Fig. 14). The application of HT layers as a surface treatment improved the adhesion of the acrylic coating to the EG steel substrate. This effect has been documented in prior studies [8,24,34]. However, the duration of the HT layer treatment showed no significant influence on the adhesion of the acrylic coating systems in this study. Amanian et al. suggested that HT conversion coatings likely increased surface roughness, which provided a larger contact area for the adhesion of organic coatings [8,34]. This enhanced surface texture promoted favorable mechanical interlocking between the HT conversion layer and the organic coatings, ultimately improving the dry adhesion of the coatings to the substrate. The HT conversion layers contain hydroxyl groups, which can interact with the various polar functional groups in the acrylic coating, forming hydrogen bonds.

Fig. 14.b–d show the optical photographs of different samples after the pull-off tests. For the EG/AC sample without HT layers (Fig. 14.b), the surface after detachment appeared relatively clean and inert, indicating predominant adhesive failure at the coating/substrate interface. In contrast, both HT-1/AC (Fig. 14.c) and HT-2/AC (Fig. 14.d) samples showed visible resin residues adhered to the substrate, suggesting a mixed or cohesive failure. This behavior can be attributed to the ability of the acrylic coating to penetrate into the voids of the HT layers, thereby increasing the effective contact area and promoting mechanical interlocking. Notably, the HT-1/AC sample retained more resin compared with HT-2/AC, suggesting stronger interfacial adhesion in the former.

Fig. 15 shows the optical photographs of acrylic coating systems after the cross-hatch adhesion test. The EG/AC sample exhibited partial coating detachment along the cuts through the coating down to the substrate, indicating weaker interfacial adhesion and local loss of cohesion (Fig. 15.a). In contrast, both coating systems with HT layers (Fig. 15.b and c) maintained well-defined lattice patterns and showed a markedly lower degree of flaking and peeling compared with EG/AC sample, confirming enhanced adhesion strength. The HT-1/AC coating showed a generally intact grid, although slight coating removal was still

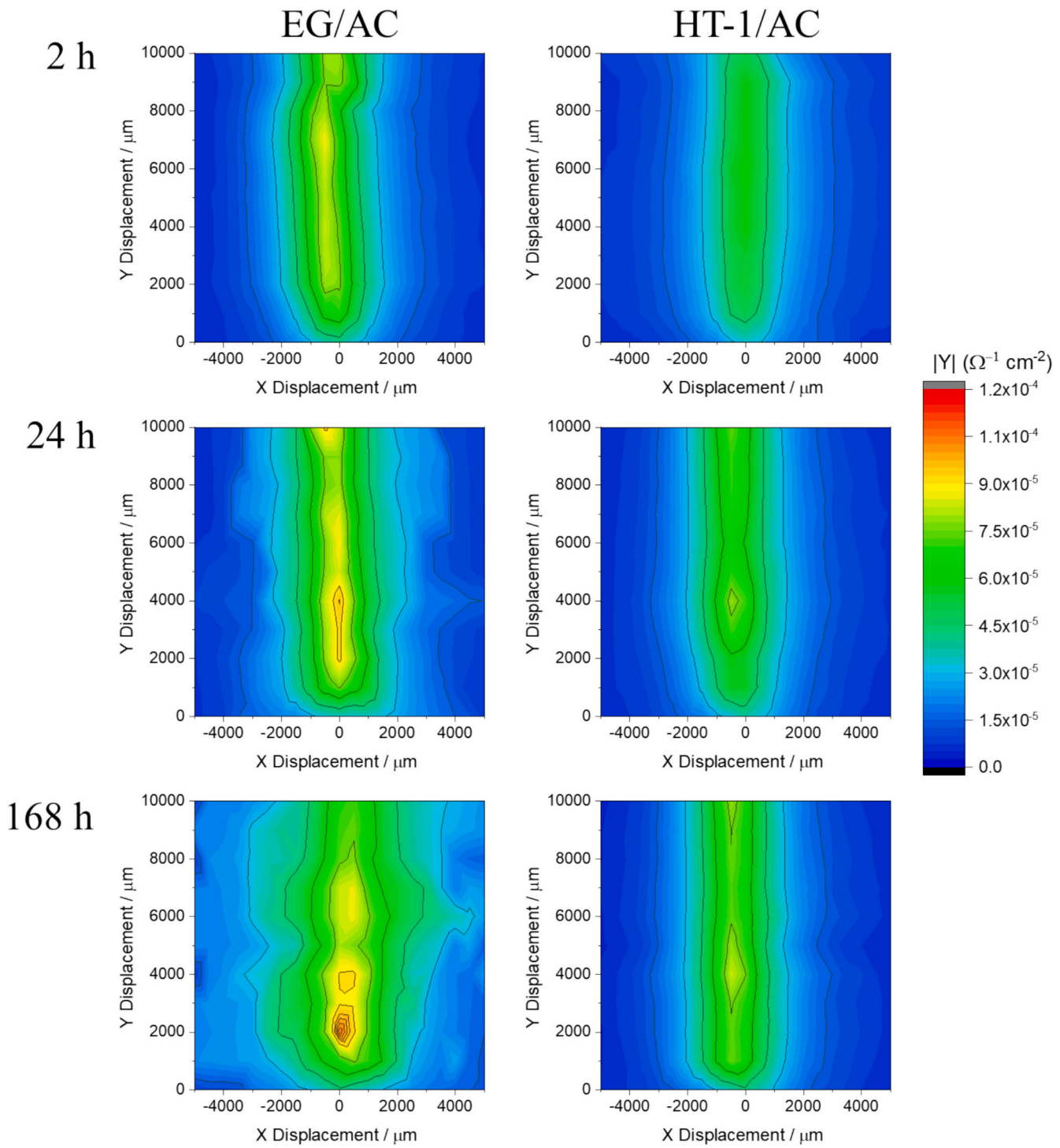

Fig. 12. LEIS mappings carried out at 1 kHz around the scratched area in 1 mM NaCl for EG/AC and HT-1/AC.

observed at some intersections. The HT-2/AC sample exhibited slightly inferior adhesion to HT-1/AC, accompanied by slight coating flaking around the scribed cuts, likely caused by micro-defects within the thicker HT layer.

Fig. 16. illustrates the visual inspection results of not scratched acrylic coating systems following 168 h salt spray test. Noticeable rust and blistered areas appeared on the acrylic coating system applied to EG steel without HT treatment layers as early as 72 h into the test (Fig. 16.a). With increased exposure time, the deterioration of the EG/AC system became severe, showing extensive "white rust" corrosion products and expanding blistered areas (Fig. 16.a). In contrast, acrylic coating systems on HT-treated samples showed minimal rust and blistering after 72 h (Fig. 16.b and c). By 168 h, the HT-2/AC system exhibited white rust corrosion and blistered areas, but the degradation was significantly less severe than the EG/AC system (Fig. 16.b). The HT-1/AC system demonstrated outstanding corrosion resistance, remaining free of degradation even after 168 h of salt spray exposure (Fig. 16.c).

4. Discussion

Consistent with previous studies on HT synthesis in alkaline environments at room temperature [8,28,35], the interlayer anions of the HT

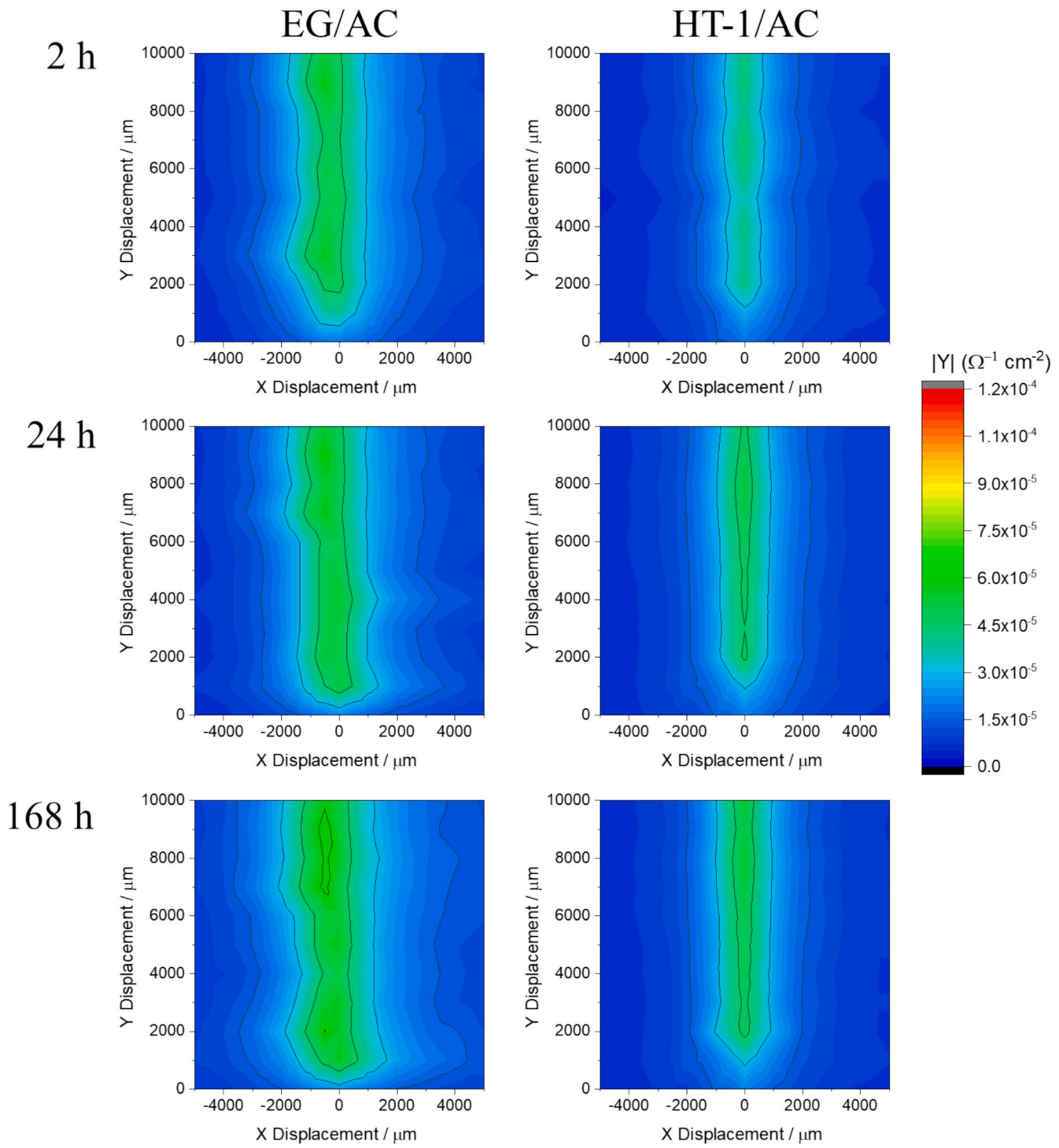

Fig. 13. LEIS mappings carried out at 1 Hz around the scratched area in 1 mM NaCl for EG/AC and HT-1/AC.

films were predominantly carbonate, originating from the dissolution of atmospheric CO_2 in the high-pH precursor solutions. XRD results confirmed that the crystal structure of the HT layers was similar irrespective of the treatment duration, indicating that synthesis time did not alter the fundamental layered double hydroxide structure. However, treatment time influenced the morphology and thickness of HT layers (Fig. 3 and Fig. 4). The prolonged treatment resulted in a thicker coating with enhanced surface coverage. This evolution can be attributed to the progressive lateral growth and stacking of HT nanosheets during extended immersion. Both EIS and polarization curves confirmed that the corrosion protection of EG steel was significantly improved by the HT conversion layers, with the sample subjected to longer treatment (HT-2) exhibiting the highest resistance. This behavior can be explained by the enhanced barrier effect of the thicker HT film, which limited the direct penetration of chloride ions to the underlying EG steel substrate and thereby delayed the corrosion process [25,29].

The role of the HT pretreatment in enhancing the performance of the acrylic topcoat was particularly noteworthy in this study. Adhesion testing showed that the presence of HT layers enhanced bond strength of the acrylic coating to substrate, attributable to increased surface roughness and hydroxylated sites that facilitate mechanical interlocking and hydrogen bonding with the polymer matrix [8,34]. The

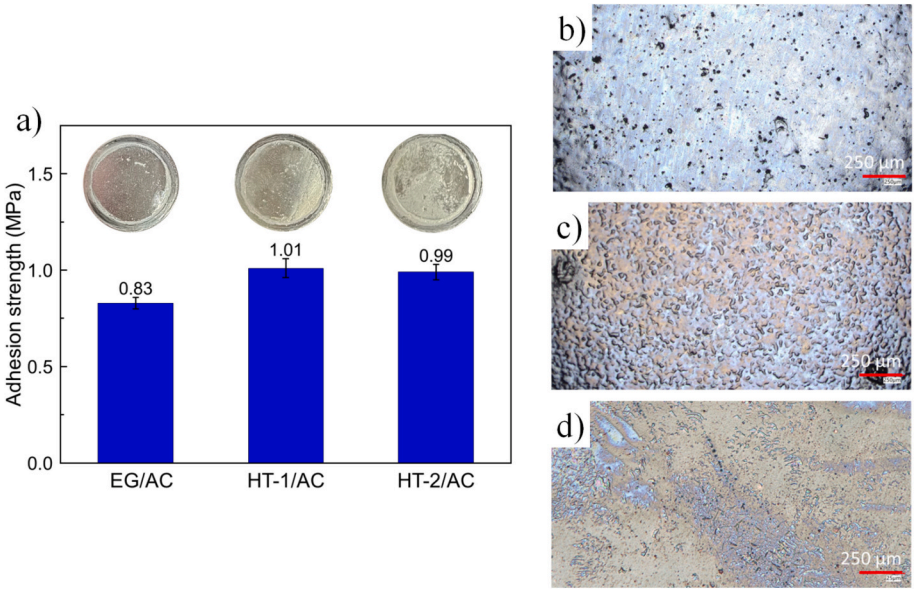

Fig. 14. (a) Adhesion strengths of acrylic coating systems, optical photographs of (b) EG/AC, (c) HT-1/AC, and (d) HT-2/AC acrylic coating systems after pull-off test.

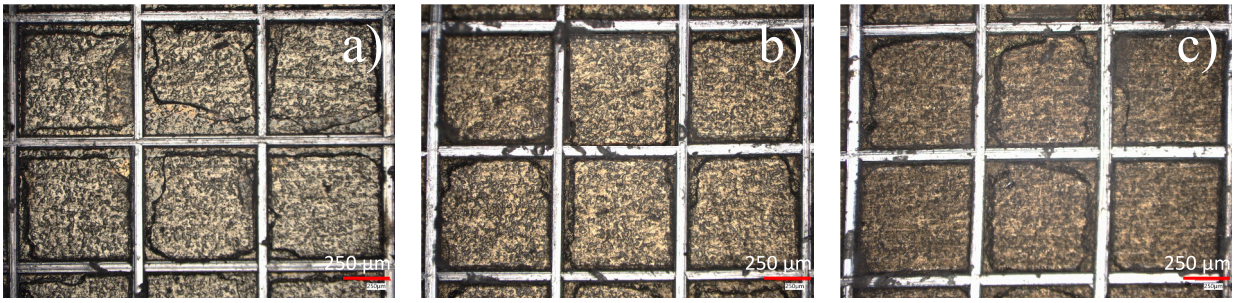

Fig. 15. The cross-hatch adhesion test images for (a) EG/AC, (b) HT-1/AC, and (c) HT-2/AC acrylic coating systems.

incorporation of HT conversion layers significantly enhanced the corrosion protection of the acrylic coating system (Fig. 9 and Fig. 15). The HT layers served as an additional barrier, restricting chloride ion mobility and delaying their direct interaction with the metal surface. Consistently, electrochemical measurements and salt spray test confirmed that the HT-1/AC system exhibited significantly delayed coating degradation compared with both bare EG and HT-2/AC. Although the HT-2 layer was thicker and provided higher intrinsic barrier protection in the absence of an organic coating, they contained loosely attached particles that introduced defects in the acrylic film, thereby enabling localized electrolyte ingress and a reduction in the global performance of coating system (Fig. 8).

Moreover, LEIS results further highlighted the protective role of the HT-1 layer in the acrylic coating system in the presence of artificial defects. Compared with the bare EG substrate, the acrylic coating system incorporating HT layer displayed markedly reduced admittance at defect sites in both high and low frequency. This demonstrated that the HT conversion layer effectively hinders the penetration of aggressive species at coating discontinuities. This finding confirmed that HT layer contributed to enhanced corrosion resistance under defect-driven degradation conditions.

These findings suggested that the HT layer with shorter pretreatment time may offer significant advantages, including improved adhesion, reduced delamination, and prolonged coating durability. These results in this research are particularly promising for future applications to enhance the corrosion protection of galvanized steel substrates, as they demonstrate that the HT conversion layer can be effectively formed at room temperature and with a reduced processing time.

5. Conclusions

In this work, ZnAl HT conversion layers with different treatment times were successfully prepared on EG steel. The treatment duration affected the corrosion protection and surface characteristics of the HT layers. The HT conversion layer with stirring for 6 h and without stirring for 16 h (HT-2) exhibited enhanced corrosion protection in 0.1 M NaCl solution. In this study, the in-situ grown HT layers significantly enhance the adhesion strength between EG steel and the top acrylic coating while also improving the corrosion resistance of the entire coating system in neutral NaCl solutions. The treatment duration of HT layers influences the corrosion protection performance of acrylic coating systems, with stirring for 2 h and without stirring for 5 h (HT-1) yielding better corrosion resistance and adhesion. In addition, LEIS results confirmed that the presence of the HT layer with shorter treatment time significantly enhanced the corrosion resistance in scratched regions of the acrylic coating system.

CRediT authorship contribution statement

Thu Thuy Pham: Writing – original draft, Validation, Methodology, Investigation, Formal analysis. **Anh Son Nguyen:** Writing – original draft, Validation, Investigation. **Yoann Paint:** Validation, Investigation.

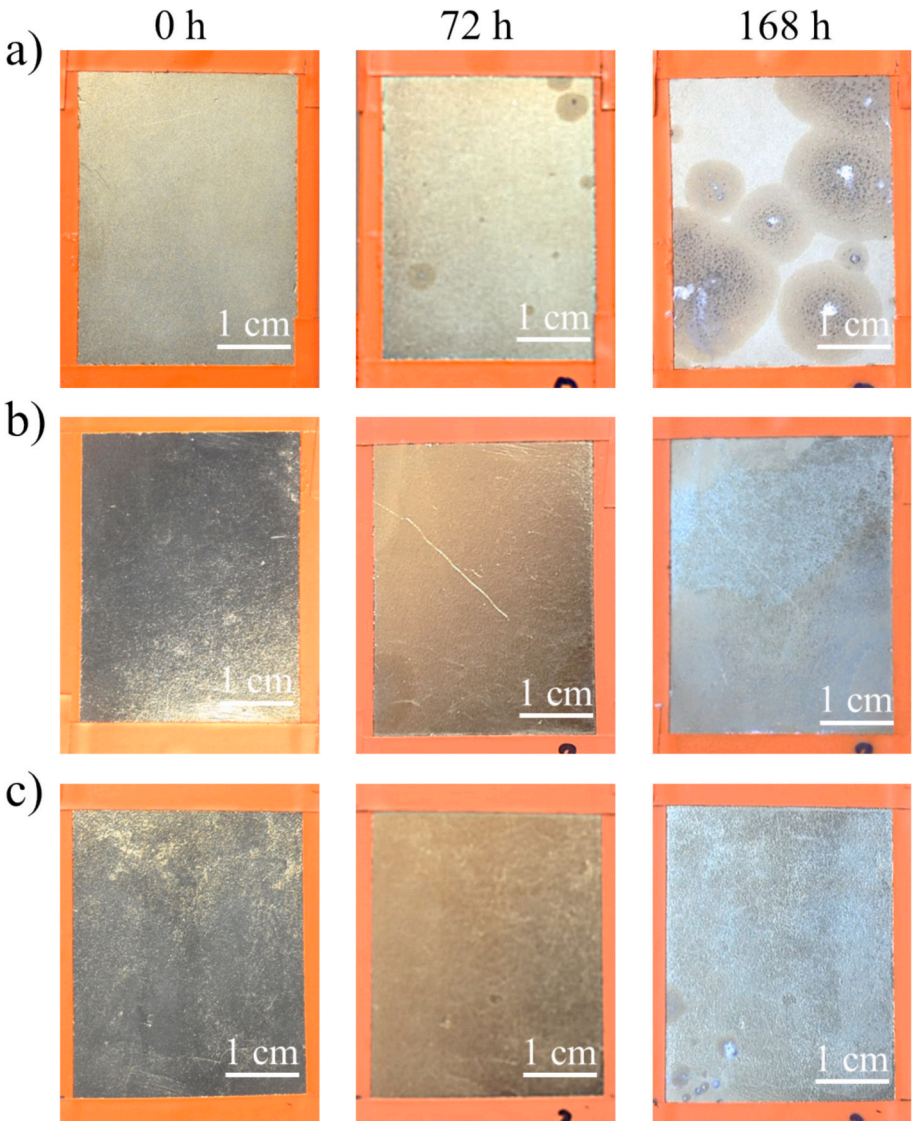

Fig. 16. Optical photographs of (a) EG/AC, (b) HT-1/AC, and (c) HT-2/AC acrylic coating systems during salt spray test.

Thuy Duong Nguyen: Validation, Investigation. **Thi Xuan Hang To:** Validation, Supervision, Methodology. **Marie-Georges Olivier:** Writing – review & editing, Supervision, Project administration, Funding acquisition, Conceptualization.

Declaration of competing interest

The authors declare that they have no known competing financial interests or personal relationships that could have appeared to influence the work reported in this paper.

Acknowledgments

This study was supported by the ARES Belgium through the Development Cooperation project between Vietnam and Belgium (PRD 2020-2025), and, Ministry of Science and Technology (Vietnam) under grant number DTDLCN.61/22.

Data availability

Data will be made available on request.

References

[1] J.L. Matos, V. Cerveira, S.M. Manhabosco, S.P.G. Valenzuela, D.P. Dick, L.F.P. Dick, Humic acid: a new corrosion inhibitor of zinc in chlorides, Electrochim. Acta 397 (2021) 139225, https://doi.org/10.1016/j.electacta.2021.139225.
[2] T.T. Pham, T.D. Nguyen, A.S. Nguyen, T.T. Nguyen, M. Gonon, A. Belfiore, Y. Paint, T.X.H. To, M.G. Olivier, Role of Al and Mg alloying elements on corrosion behavior of zinc alloy-coated steel substrates in 0.1 M NaCl solution, Mater. Corros. (2023) 903–919, https://doi.org/10.1002/maco.202213549.
[3] M.A. Iqbal, H. Asghar, M. Mohedano, M. Fedel, Development of superhydrophobic layered double hydroxide directly on zinc substrate: structural and corrosion resistance properties, Bull. Mater. Sci. 46 (2023), https://doi.org/10.1007/s12034-023-03055-6, 46:215.
[4] P.K. Rai, D. Rout, D. Satish Kumar, S. Sharma, G. Balachandran, Effect of magnesium on corrosion behavior of hot-dip Zn-Al-Mg coating, J. Mater. Eng. Perform. 30 (2021) 4138–4147, https://doi.org/10.1007/s11665-021-05718-z.
[5] N. Taleghani, M.M. Attar, Corrosion, physical characters, and synergetic effects of SAPP and SM in polyurethane coating on galvanized steel, Chem. Pap. 77 (2022) 1497–1506, https://doi.org/10.1007/s11696-022-02525-1.
[6] A. Cristoforetti, S. Rossi, F. Deflorian, M. Fedel, Comparative study between natural and artificial weathering of acrylic-coated steel, aluminum, and galvanized steel, Mater. Corros. 74 (2023) 1429–1438, https://doi.org/10.1002/maco.202313858.
[7] J. Rodriguez, E. Bollen, T.D. Nguyen, A. Portier, Y. Paint, M.G. Olivier, Incorporation of layered double hydroxides modified with benzotriazole into an epoxy resin for the corrosion protection of Zn-Mg coated steel, Prog. Org. Coat. 149 (2020) 105894, https://doi.org/10.1016/j.porgcoat.2020.105894.
[8] S. Amanian, R. Naderi, M. Mahdavian, The role of an in-situ grown Zn-Al layered double hydroxide conversion coating in the protective properties of epoxy coating

on galvanized steel, J. Electrochem. Soc. 169 (2022) 031511, https://doi.org/10.1149/1945-7111/ac5d95.
[9] Z. Gao, D. Zhang, X. Li, S. Jiang, Q. Zhang, Current status, opportunities and challenges in chemical conversion coatings for zinc, Colloids Surf. A Physicochem. Eng. Asp. 546 (2018) 221–236, https://doi.org/10.1016/j.colsurfa.2018.03.018.
[10] X. Zhang, W.G. Sloof, A. Hovestad, E.P.M. van Westing, H. Terryn, J.H.W. de Wit, Characterization of chromate conversion coatings on zinc using XPS and SKPFM, Surf. Coat. Technol. 197 (2005) 168–176, https://doi.org/10.1016/j.surfcoat.2004.08.196.
[11] C.R. Tomachuk, C.I. Elsner, A.R. Di Sarli, O.B. Ferraz, Morphology and corrosion resistance of Cr(III)-based conversion treatments for electrogalvanized steel, J. Coat. Technol. Res. 7 (2009) 493–502, https://doi.org/10.1007/s11998-009-9213-1.
[12] J. Yang, K. Dong, Y. Song, X. Cheng, E.-H. Han, Study on the phosphate/electrophoretic composite coatings on Mg alloy: the effect of phosphate conversion films on adhesion strength and corrosion resistance, Surf. Coat. Technol. 489 (2024) 131109, https://doi.org/10.1016/j.surfcoat.2024.131109.
[13] H. Asemani, P. Ahmadi, A. Sarabi, H.E. Mohammadloo, Effect of zirconium conversion coating: adhesion and anti-corrosion properties of epoxy organic coating containing zinc aluminum polyphosphate (ZAPP) pigment on carbon mild steel, Prog. Org. Coat. 94 (2016) 18–27, https://doi.org/10.1016/j.porgcoat.2016.01.015.
[14] M. Fedel, M.-E. Druart, M. Olivier, M. Poelman, F. Deflorian, S. Rossi, Compatibility between cataphoretic electro-coating and silane surface layer for the corrosion protection of galvanized steel, Prog. Org. Coat. 69 (2010) 118–125, https://doi.org/10.1016/j.porgcoat.2010.04.003.
[15] T.T. Pham, T.D. Nguyen, A.S. Nguyen, M. Gonon, A. Belfiore, Y. Paint, T.X. Hang To, M.-G. Olivier, Influence of solution pH on the structure formation and protection properties of ZnAlCe hydrotalcites layers on hot-dip galvanized steel, Surf. Coat. Technol. 472 (2023) 129918, https://doi.org/10.1016/j.surfcoat.2023.129918.
[16] P. Savignac, M.J. Menu, M. Gressier, B. Denat, Y.E. Khadir, S. Manov, F. Ansart, Improvement of adhesion properties and corrosion resistance of sol-gel coating on zinc, Molecules 23 (2018) 1079, https://doi.org/10.3390/molecules23051079.
[17] G. Kong, L. Lingyan, J. Lu, C. Che, Z. Zhong, Corrosion behavior of lanthanum-based conversion coating modified with citric acid on hot dip galvanized steel in aerated 1M NaCl solution, Corros. Sci. 53 (2011) 1621–1626, https://doi.org/10.1016/j.corsci.2011.01.038.
[18] X. Feng, R. Long, L. Wang, C. Liu, Z. Bai, X. Liu, A review on heavy metal ions adsorption from water by layered double hydroxide and its composites, Sep. Purif. Technol. 284 (2022) 120099, https://doi.org/10.1016/j.seppur.2021.120099.
[19] Y. Cao, D. Zheng, F. Zhang, J. Pan, C. Lin, Layered double hydroxide (LDH) for multi-functionalized corrosion protection of metals: a review, J. Mater. Sci. Technol. 102 (2022) 232–263, https://doi.org/10.1016/j.jmst.2021.05.078.
[20] J. Stephan, V. Kasneryk, M. Serdechnova, N. Scharnagl, E. Gazenbiller, B. Vaghefinazari, P. Volovitch, M. Starykevich, C. Blawert, M.L. Zheludkevich, Formation of Li-Al LDH conversion layer on AA2024 alloy for corrosion protection, Appl. Surf. Sci. 659 (2024) 159919, https://doi.org/10.1016/j.apsusc.2024.159919.
[21] M. Hao, H. Tan, W. Yang, D. Yue, L. Gao, Z. Wang, C. He, Effect of pH on long-term corrosion protection of Zn doped MgAl-LDHs coatings by in situ growth on 5052 aluminum alloy, Surf Interfaces 64 (2025) 106349, https://doi.org/10.1016/j.surfin.2025.106349.
[22] J. Cao, Y. Wu, W. Zhao, Review of layered double hydroxide (LDH) nanosheets in corrosion mitigation: recent developments, challenges, and prospects, Materials 18 (2025), https://doi.org/10.3390/ma18061190.
[23] T.D. Nguyen, A.S. Nguyen, B.A. Tran, K.O. Vu, D.L. Tran, T.T. Phan, N. Scharnagl, M.L. Zheludkevich, T.X.H. To, Molybdate intercalated hydrotalcite/graphene oxide composite as corrosion inhibitor for carbon steel, Surf. Coat. Technol. 399 (2020) 126165, https://doi.org/10.1016/j.surfcoat.2020.126165.
[24] T. Xu, L. Yu, J.-M. Hu, In-situ Zn-Al layered double hydroxide conversion coatings prepared on galvanized steels by a two-step electrochemical method, Corros. Sci. 233 (2024) 112057, https://doi.org/10.1016/j.corsci.2024.112057.
[25] T. Thi Xuan Hang, T.T. Pham, T.D. Nguyen, M.-G. Olivier, A review: Hydrotalcite layers as protective coatings on zinc and zinc alloys, Vietnam J. Sci. Technol. 62 (2024) 1047–1064, https://doi.org/10.15625/2525-2518/21045.
[26] L. Guo, W. Wu, Y. Zhou, F. Zhang, R. Zeng, J. Zeng, Layered double hydroxide coatings on magnesium alloys: a review, J. Mater. Sci. Technol. 34 (2018) 1455–1466, https://doi.org/10.1016/j.jmst.2018.03.003.
[27] A.C. Bouali, M. Serdechnova, C. Blawert, J. Tedim, M.G.S. Ferreira, M. L. Zheludkevich, Layered double hydroxides (LDHs) as functional materials for the corrosion protection of aluminum alloys: a review, Appl. Mater. Today 21 (2020) 100857, https://doi.org/10.1016/j.apmt.2020.100857.
[28] K. Hoshino, S. Furuya, R.G. Buchheit, Effect of solution pH on layered double hydroxide formation on electrogalvanized steel sheets, J. Mater. Eng. Perform. 28 (2019) 2237–2244, https://doi.org/10.1007/s11665-019-03963-x.
[29] T.T. Pham, T.D. Nguyen, A.S. Nguyen, M. Gonon, X. Noirfalise, Y. Paint, T.X.H. To, M.-G. Olivier, Study of the formation and anti-corrosion properties of Zn Al hydrotalcite conversion films grown “in situ” on different zinc alloys coated steel, Prog. Org. Coat. 173 (2022) 107221, https://doi.org/10.1016/j.porgcoat.2022.107221.
[30] A. Mikhailau, H. Maltanava, S.K. Poznyak, A.N. Salak, M.L. Zheludkevich, K. A. Yasakau, M.G.S. Ferreira, One-step synthesis and growth mechanism of nitrate intercalated ZnAl LDH conversion coatings on zinc, Chem. Commun. 55 (2019) 6878–6881, https://doi.org/10.1039/C9CC02571E.
[31] Q. Huang, Y. Wang, B. Zhou, Y. Wei, F. Gao, T. Fujita, The effect of ZnAl-LDHs-CO_3 on the corrosion behaviour of Zn-5Al alloys in 3.5wt.% NaCl solution, Corros. Sci. 179 (2021) 109165, https://doi.org/10.1016/j.corsci.2020.109165.
[32] K.A. Yasakau, A. Kuznetsova, H.M. Maltanava, S.K. Poznyak, M.G.S. Ferreira, M. L. Zheludkevich, Corrosion protection of zinc by LDH conversion coatings, Corros. Sci. 229 (2024) 11889, https://doi.org/10.1016/j.corsci.2024.111889.
[33] A.C. Bouali, M.H. Iuzviuk, M. Serdechnova, K.A. Yasakau, D.C.F. Wieland, G. Dovzhenko, H. Maltanava, I.A. Zobkalo, M.G.S. Ferreira, M.L. Zheludkevich, Zn-Al LDH growth on AA2024 and zinc and their intercalation with chloride: comparison of crystal structure and kinetics, Appl. Surf. Sci. 501 (2020) 144027, https://doi.org/10.1016/j.apsusc.2019.144027.
[34] S. Amanian, R. Naderi, M. Mahdavian, Benzotriazole modified Zn-Al layered double hydroxide conversion coating on galvanized steel for improved corrosion resistance, J. Taiwan Inst. Chem. Eng. 150 (2023) 105072, https://doi.org/10.1016/j.jtice.2023.105072.
[35] T.T. Pham, T.D. Nguyen, A.S. Nguyen, Y. Paint, M. Gonon, T.X.H. To, M.-G. Olivier, A comparative study of the structure and corrosion resistance of ZnAl hydrotalcite conversion layers at different Al^{3+}/Zn^{2+} ratios on electrogalvanized steel, Surf. Coat. Technol. 429 (2022) 127948, https://doi.org/10.1016/j.surfcoat.2021.127948.
[36] D.T. Nguyen, H.T.X. To, J. Gervasi, Y. Paint, M. Gonon, M.-G. Olivier, Corrosion inhibition of carbon steel by hydrotalcites modified with different organic carboxylic acids for organic coatings, Prog. Org. Coat. 124 (2018) 256–266, https://doi.org/10.1016/j.porgcoat.2017.12.006.
[37] N.T.T. Huong, L.D. Bao, L.B. Thang, N. Van Chien, T.T. Nam, N. Van Khuong, Corrosion behavior of electrodeposited ZnNi alloy–CeO_2 modified SiO_2 particle composite coatings, Russ. J. Phys. Chem. A 95 (2021) 827–833.
[38] Y. Meng, L. Liu, D. Zhang, C. Dong, Y. Yan, A.A. Volinsky, L.N. Wang, Initial formation of corrosion products on pure zinc in saline solution, Bioact. Mater 4 (2019) 87–96, https://doi.org/10.1016/j.bioactmat.2018.08.003.
[39] Y. Tang, F. Wu, L. Fang, T. Guan, J. Hu, S. Zhang, A comparative study and optimization of corrosion resistance of ZnAl layered double hydroxides films intercalated with different anions on AZ31 Mg alloys, Surf. Coat. Technol. 358 (2019) 594–603, https://doi.org/10.1016/j.surfcoat.2018.11.070.
[40] Y. Ye, D. Yang, D. Zhang, H. Chen, H. Zhao, X. Li, L. Wang, POSS-tetraaniline modified graphene for active corrosion protection of epoxy-based organic coating, Chem. Eng. J. 383 (2020) 123160, https://doi.org/10.1016/j.cej.2019.123160.
[41] Y. Ye, D. Yang, H. Chen, S. Guo, Q. Yang, L. Chen, H. Zhao, L. Wang, A high-efficiency corrosion inhibitor of N-doped citric acid-based carbon dots for mild steel in hydrochloric acid environment, J. Hazard. Mater. 381 (2020) 121019, https://doi.org/10.1016/j.jhazmat.2019.121019.
[42] K. Sarkar, Amerjit, R. Raj, T.K. Rout, S. Bose, A ‘tortuous path’ and ‘protective oxide layer’ work in tandem in unique corrosion-resistant polyetherimide coatings, RSC Appl. Interfaces 1 (2024) 958–976, https://doi.org/10.1039/D4LF00028E.
[43] A.S. Nguyen, N. Pébère, A local electrochemical impedance study of the self-healing properties of waterborne coatings on 2024 aluminium alloy, Electrochim. Acta 222 (2016) 1806–1817, https://doi.org/10.1016/j.electacta.2016.11.152.